Flow Measurement and Instrumentation 37 (2014) 107–118

Contents lists available at ScienceDirect

Flow Measurement and Instrumentation

journal homepage: www.elsevier.com/locate/flowmeasinst

A review of the theory of Coriolis flowmeter measurement errors due to entrained particles

Nils T. Basse

Siemens A/S, Flow Instruments, Nordborgvej 81, 6430 Nordborg, Denmark

ARTICLE INFO

Article history:
Received 6 November 2013
Received in revised form
17 March 2014
Accepted 31 March 2014
Available online 13 April 2014

Keywords:
Coriolis flowmeters
Two-phase flow
Flow measurement errors
Bubble theory
Compressibility

ABSTRACT

Coriolis flowmeters operate with high accuracy when the medium metered is a single-phase incompressible fluid. Multi-phase fluids lead to measurement errors because of center-of-mass motion. In this paper we review the "bubble theory" which describes errors due to phase decoupling of two-phase fluids. Examples are provided with combined phase decoupling and compressibility errors.

1. Introduction

For normal operation of Coriolis flowmeters, the mass flow rate and density of the fluid is measured under the assumption that the center-of-mass (CM) is fixed on the axis of the vibrating pipe(s).

This assumption of a fixed CM is violated if either compressibility or phase decoupling occurs [1]. An overview of the relevance of these effects is provided in Table 1.

The measurement errors due to compressibility increase with decreasing speed of sound and are always positive: the measurement is above the true value [2]. The physical reason for the moving CM is that transverse acoustic modes (pressure waves) are excited. This excitation can occur even if the pipes are not vibrated by external means. Compressibility effects are most severe when the frequency of the fundamental transverse acoustic mode (FTAM) approaches the driver frequency.

Errors due to phase decoupling occur because the acceleration of the two phases is different. "Bubble theory" is a theoretical treatment of errors due to phase decoupling [3,4]. For this error type, measurement errors are negative, i.e. measurements are below the true value.

Models including effects due to both phase decoupling and compressibility can be found in [5,6].

Additional effects which may cause measurement errors have been identified, e.g., asymmetric damping [7,8] and velocity profile [9,10]. These effects are outside the scope of this paper.

Representative examples of Coriolis measurement errors for two- and three-phase flows can be found in [11,12].

Nomenclature: a fluid is either a liquid or a gas. A particle can be either a solid or a fluid (gas bubble or liquid droplet).

To date, the published bubble theory has dealt with zero particle density combined with either viscous or inviscid fluids. A direct comparison of the bubble theory with measurements for an air–water mixture can be found in [4].

In this paper, we review the complete bubble theory, which includes effects associated with finite particle density and viscosity.

The paper is organized as follows: In Section 2 we study the dynamics of an infinitely viscous particle immersed in an inviscid fluid. In Section 3 we derive the force on a vibrating container due to inviscid particles having finite density in an inviscid fluid. This is followed by a brief review of the case of a viscous fluid with zero density particles in Section 4. The complete expression, which includes finite particle density and viscosity, is presented in Section 5. Mass flow rate and density measurement errors due to phase decoupling are derived in Section 6. Compressibility errors are briefly summarized in Section 7 and combined measurement errors due to both compressibility and phase decoupling can be found in Section 8. The most important assumptions and limitations of the bubble theory are discussed in Section 9. Finally, we summarize our conclusions in Section 10.

2. Infinitely viscous particle and inviscid fluid: finite particle density

2.1. Virtual mass of particle

We begin this Section by reviewing the virtual mass of a particle in a fluid, see § 11 in [13].

E-mail address: nils.basse@siemens.com

http://dx.doi.org/10.1016/j.flowmeasinst.2014.03.009
0955-5986/

Table 1
Overview of measurement errors.

Phase	Compressibility error	Phase decoupling error
Liquid	Small	Not applicable
Gas	Medium	Not applicable
Two-phase (e.g., gas and liquid)	Large	Large

We consider a particle exhibiting oscillatory motion in a fluid under the influence of an external force $\bar{f}$. We wish to find the equation of motion of the particle.

The momentum of the particle is

$$\bar{p}_p = m_p \bar{u}_p, \tag{1}$$

where the subscript "p" is the particle, $\bar{p}$ is the momentum, m is the mass and $\bar{u}$ is the velocity.

The momentum of the fluid is

$$\bar{p}_f = m_{induced} \bar{u}_p, \tag{2}$$

where the subscript "f" is the fluid and $m_{induced}$ is the induced mass (in general: the induced-mass tensor m_{ik}).

The temporal derivative of the total momentum of the system is equal to the external force

$$\bar{f} = \frac{d(\bar{p}_p + \bar{p}_f)}{dt} = (m_p + m_{induced})\frac{d\bar{u}_p}{dt} = \bar{f}_p + \bar{f}_f \tag{3}$$

The force on the particle due to the fluid ($\bar{f}_f$) exists because the particle has to displace some volume of the surrounding fluid, i.e. the fluid exerts a drag force on the particle. The additional inertia of the system can be modeled as a part of the fluid moving with the particle.

The equation of motion of the particle is

$$\bar{f} = (m_p + m_{induced})\frac{d\bar{u}_p}{dt} = m_{virtual}\frac{d\bar{u}_p}{dt}, \tag{4}$$

where

$$m_{virtual} = m_p + m_{induced} \tag{5}$$

is the virtual mass of the particle.

An alternative nomenclature can also be found in the literature

$$m_{effective} = m_p + m_{added} \tag{6}$$

2.1.1. Example: spherical particle

We assume the particle to be a sphere having radius a and volume

$$V_p = \tfrac{4}{3}\pi a^3 \tag{7}$$

The actual mass of the sphere is

$$m_p = \rho_p V_p, \tag{8}$$

where ρ is density and the induced mass is [14]

$$m_{induced} = \frac{2}{3}\pi\rho_f a^3 = \frac{1}{2}\rho_f V_p \tag{9}$$

Then we can write the equation of motion for a sphere exhibiting oscillatory motion in a fluid

$$\bar{f} = \left(\rho_p + \frac{1}{2}\rho_f\right) V_p \frac{d\bar{u}_p}{dt} \tag{10}$$

For this example, the induced mass is half of the mass of the fluid displaced by the sphere.

2.2. Particle velocity

We continue by considering the particle velocity, also based on § 11 in [13].

Here, we study a particle set in motion by an oscillating fluid. We wish to find an equation for the particle velocity.

First consider the situation where the particle is carried along with the fluid ($\bar{u}_f = \bar{u}_p$). Under this assumption, the force acting on the particle is

$$\bar{f}_p|_{\bar{u}_f = \bar{u}_p} = \rho_f V_p \frac{d\bar{u}_f}{dt} = \rho_f V_p \bar{a}_f \tag{11}$$

Next consider motion of the particle relative to the fluid. This motion leads to an additional reactive force on the particle (see Eq. (3))

$$\bar{f}_p|_{\bar{u}_f \neq \bar{u}_p} = -m_{induced}\frac{d(\bar{u}_p - \bar{u}_f)}{dt} \tag{12}$$

So the total force on the particle is

$$\bar{f}_p = \bar{f}_p|_{\bar{u}_f = \bar{u}_p} + \bar{f}_p|_{\bar{u}_f \neq \bar{u}_p} = \rho_f V_p \bar{a}_f - m_{induced}\frac{d(\bar{u}_p - \bar{u}_f)}{dt} \tag{13}$$

The total force can also be expressed as the derivative with respect to time of the particle momentum

$$\frac{d}{dt}(\rho_p V_p \bar{u}_p) = \bar{f}_p = \rho_f V_p \bar{a}_f - m_{induced}\frac{d(\bar{u}_p - \bar{u}_f)}{dt} \tag{14}$$

Rearranging terms we find

$$\frac{d\bar{u}_p}{dt}(\rho_p V_p + m_{induced}) = \frac{d\bar{u}_f}{dt}(\rho_f V_p + m_{induced}) \tag{15}$$

and integrating both sides with respect to time

$$\bar{u}_p(\rho_p V_p + m_{induced}) = \bar{u}_f(\rho_f V_p + m_{induced}) \tag{16}$$

The expression for the particle velocity is

$$\bar{u}_p = \bar{u}_f\left(\frac{\rho_f V_p + m_{induced}}{\rho_p V_p + m_{induced}}\right) \tag{17}$$

2.2.1. Example: spherical particle

Again we assume that the particle is a sphere. The equation for the velocity of the sphere is

$$\bar{u}_p = \bar{u}_f \frac{3\rho_f}{2\rho_p + \rho_f} \tag{18}$$

Three cases can be considered:

For a high density sphere the velocity of the sphere is zero

$$\begin{aligned} &\rho_f \ll \rho_p \\ &\bar{u}_p \approx 0 \end{aligned} \tag{19}$$

For identical fluid and particle densities, the velocities are the same

$$\begin{aligned} &\rho_f = \rho_p \\ &\bar{u}_p = \bar{u}_f \end{aligned} \tag{20}$$

For a low density sphere, the velocity of the sphere is three times higher than the fluid velocity

$$\begin{aligned} &\rho_f \gg \rho_p \\ &\bar{u}_p \approx 3\bar{u}_f \end{aligned} \tag{21}$$

From this example we see that the velocity (and acceleration) of the particle and the fluid can differ. This leads to the phase decoupling phenomenon.

3. Inviscid particle and fluid: finite particle density

We now proceed to derive the force on an oscillating container due to a particle.

The major part of the derivation in this Section was taken from [15].

In the remainder of this paper we will assume that the particle is a sphere.

3.1. Motion of container and particle

We use spherical and Cartesian coordinate systems as defined in Fig. 1.

We study motion of a particle in a fluid. The fluid is in a rigid container with surface area S_f. The container oscillates in the z direction with acceleration a_c, see the sketch in Fig. 1. The particle inside the container has a surface area S_p.

The particle is assumed to be far from the wall of the container. This is used when deriving the near flow field of the particle. An equivalent assumption is that the particle size is small relative to the size of the container.

The container oscillates at an angular frequency ω with a small amplitude ξ (small compared to the particle radius). This assumption allows us to neglect the non-linear term in the Navier–Stokes equations, and is also needed for the boundary condition on the particle surface. The small amplitude oscillation also means that the particle maintains its spherical shape, i.e. surface tension does not have to be taken into account.

The effect of gravity is neglected. If gravity were included, it would cause a small drifting velocity of the particles superimposed onto their vibrating motion. Thus they would sink or rise at a rate which is assumed to be slow compared to their velocity through the flowmeter.

$$\begin{aligned} z &= \xi e^{i\omega t} \\ u &= \frac{dz}{dt} = i\omega z \\ a_c &= \frac{du}{dt} = i\omega u = -\omega^2 z \end{aligned} \tag{22}$$

We work with coordinates fixed with respect to the container. Since the container is oscillating (accelerating), it is not an inertial frame. Therefore, we must include a fictitious force, the inertia force density (χ_f and χ_p) in the equations of motion for the fluid and the particle respectively.

The equation of motion of the fluid in the container is

$$\begin{aligned} i\omega\rho_f \overline{u}_f &= -\nabla P_f + \chi_f \hat{z} \\ \chi_f &= -\rho_f a_c, \end{aligned} \tag{23}$$

where P is the total pressure and $\hat{z}$ is a unit vector in the z direction.

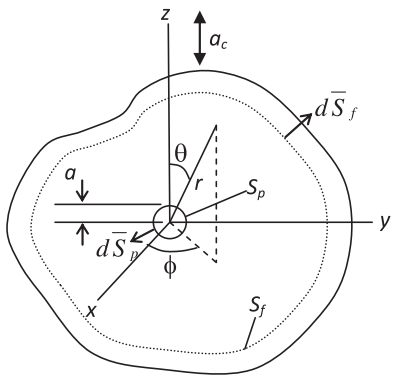

Fig. 1. Container and particle geometry, adapted from [16].

The equation of motion of the material in the particle is

$$\begin{aligned} i\omega\rho_p \overline{u}_p &= -\nabla P_p + \chi_p \hat{z} \\ \chi_p &= -\rho_p a_c \end{aligned} \tag{24}$$

If the density of the fluid and particle is the same, the pressure in the particle and in the fluid is the same

$$\begin{aligned} \rho_p &= \rho_f \\ \chi_p &= \chi_f \\ \overline{u}_f &= 0 \\ \overline{u}_p &= 0 \\ P_f &= p_{f,0} = \chi_f z \\ P_p &= p_{p,0} = \chi_f z \end{aligned} \tag{25}$$

3.2. Expression for the additional force on the container that occurs when the densities of fluid and particle differ

If the densities of fluid and particle differ, the pressures and velocities also differ

$$\begin{aligned} \rho_p &\neq \rho_f \\ P_f &= p_{f,0} + p_f \\ P_p &= p_{f,0} + p_p \\ p_{f,0} &= \chi_f z \\ i\omega\rho_f \overline{u}_f &= -\nabla p_f \\ i\omega\rho_p \overline{u}_p &= -\nabla p_p + (\chi_p - \chi_f)\hat{z} \end{aligned} \tag{26}$$

This results in an extra force on the container due to the pressure on the inside surface S_f is associated with the relative motion of the particle and the fluid.

We now calculate this extra force in the z direction on the container due to the density difference

$$F_{f,z} = \oint_{S_f} p_f dS_{f,z} \tag{27}$$

We can use the divergence theorem to convert between volume and surface integrals

$$\int_{V_f} \nabla p_f dV_f = \oint_{S_f} p_f d\overline{S}_f \tag{28}$$

We apply this to the fluid in the container surrounding the particle

$$\begin{aligned} \nabla p_f &= -i\omega\rho_f \overline{u}_f \\ \int_{V_f} \nabla p_f dV_f &= -i\omega\rho_f \int_{V_f} \overline{u}_f dV_f = \oint_{S_f} p_f d\overline{S}_f - \oint_{S_p} p_f d\overline{S}_p \end{aligned} \tag{29}$$

Using suffix notation (i=1, 2 and 3) we can write this as

$$-i\omega\rho_f \int_{V_f} u_{f,i} dV_f = \oint_{S_f} p_f dS_{f,i} - \oint_{S_p} p_f dS_{p,i} \tag{30}$$

Further, we introduce the Einstein summation convention (sum over repeated indices) and rewrite the velocity as a divergence

$$u_{f,i} = \frac{\partial}{\partial x_{f,k}}(x_{f,i} u_{f,k}) = x_{f,i}\frac{\partial u_{f,k}}{\partial x_{f,k}} + u_{f,k}\frac{\partial x_{f,i}}{\partial x_{f,k}} = u_{f,k}\frac{\partial x_{f,i}}{\partial x_{f,k}} = u_{f,k}\delta_{ik}, \tag{31}$$

where δ_{ik} is the Kronecker delta, and the fluid is assumed to be incompressible

$$\frac{\partial u_{f,k}}{\partial x_{f,k}} = \nabla \cdot \overline{u}_f = 0 \tag{32}$$

We can express the velocity integrated over the container volume as a surface integral over the particle

$$\int_{V_f} u_{f,i}dV_f = \int_{V_f}\left(\frac{\partial}{\partial x_{f,k}}(x_{f,i}u_{f,k})\right)dV_f$$
$$= \oint_{S_f} x_{f,i}u_{f,k}dS_{f,k} - \oint_{S_p} x_{f,i}u_{f,k}dS_{p,k} = -\oint_{S_p} x_{f,i}u_{f,k}dS_{p,k}, \quad (33)$$

since

$$u_{f,k}dS_{f,k} = \overline{u}_f \cdot d\overline{S}_f = 0 \quad (34)$$

Finally, we have an expression for the force as a sum of two surface integrals over the particle

$$F_{f,z} = \oint_{S_f} p_f\, dS_{f,z} = \oint_{S_p} p_f dS_{p,z} - i\omega\rho_f \int_{V_f} u_{f,z}dV_f$$
$$= \oint_{S_p} p_f dS_{p,z} + i\omega\rho_f \oint_{S_p} z u_{f,r}dS_p \quad (35)$$

3.3. Expressions for pressure and velocity

In our derivation, we still have to calculate the pressure and velocity close to the particle.

The equations of motion are given by Eq. (26).

On the surface of the particle ($r = a$), the pressure and the radial velocity of the fluid and particle are equal

$$p_f = p_p|_{r=a}$$
$$u_{f,r} = u_{p,r}|_{r=a} \quad (36)$$

We assume that the velocity in the fluid and in the particle is divergence free (i.e. incompressible)

$$\nabla^2 p_f = \nabla^2 p_p = 0 \quad (37)$$

We now use spherical coordinates fixed at the center of the particle, where the distance from the center of the particle is r, see Fig. 1.

Possible solutions for the pressures are then

$$p_p = Kr\ \cos\ \theta$$
$$p_f = \frac{B}{r^2}\cos\ \theta, \quad (38)$$

where K and B are constants. The radial derivative of the pressure in the particle and fluid is

$$\frac{\partial p_p}{\partial r} = K\ \cos\ \theta$$
$$\frac{\partial p_f}{\partial r} = -\frac{2B}{r^3}\cos\ \theta \quad (39)$$

Eq. (26) leads us to the equations of motion for the radial velocity components

$$i\omega\rho_p u_{p,r} = -K\ \cos\ \theta + (\chi_p - \chi_f)\cos\ \theta$$
$$i\omega\rho_f u_{f,r} = \frac{2B\ \cos\ \theta}{r^3} \quad (40)$$

To determine the equation relating constants K and B, we consider the pressure on the particle surface

$$p_f = p_p|_{r=a} \Rightarrow Ka = \frac{B}{a^2}$$
$$B = a^3K \quad (41)$$

The expression for K is derived from the radial velocity on the particle surface

$$u_{f,r} = u_{p,r}|_{r=a} \Rightarrow \frac{-K+\chi_p-\chi_f}{\rho_p} = \frac{2K}{\rho_f}$$
$$K\left(\frac{2\rho_p}{\rho_f}+1\right) = \chi_p - \chi_f = a_c(\rho_f - \rho_p)$$
$$K = a_c\rho_f\left(\frac{\rho_f-\rho_p}{2\rho_p+\rho_f}\right) \quad (42)$$

3.4. Combining expressions for pressure and velocity with the additional force on the container

We now combine the results from Sections 3.2 and 3.3 to derive an expression for the additional force as a function of the densities of the fluid and particle.

The area of a strip on the surface of the particle is

$$dS_p = r\,d\theta\,2\pi r\ \sin\ \theta|_{r=a} = 2\pi a^2\ \sin\ \theta\,d\theta \quad (43)$$

The projection of the strip onto the z coordinate is

$$dS_{p,z} = \cos\ \theta\,dS_p = 2\pi a^2\ \sin\ \theta\ \cos\ \theta\,d\theta \quad (44)$$

We are now in a position to derive the desired expression for the additional force on the container:

$$F_{f,z} = \oint_{S_f} p_f\, dS_{f,z} = \oint_{S_p} p_f\, dS_{p,z} + i\omega\rho_f \oint_{S_p} z u_{f,r}\, dS_p$$
$$= \oint_{S_p} p_f\, dS_{p,z} + i\omega\rho_f \oint_{S_p} (ru_{f,r})|_{r=a}\, dS_{p,z}$$
$$= \oint_{S_p} p_f 2\pi a^2\ \sin\ \theta\ \cos\ \theta\,d\theta + i\omega\rho_f \oint_{S_p} (ru_{f,r})|_{r=a} 2\pi a^2\ \sin\ \theta\ \cos\ \theta\,d\theta$$
$$= 2\pi a^2 \int_0^\pi \left(\frac{B\cos^2\theta\ \sin\ \theta}{a^2} + \frac{2B\cos^2\theta\ \sin\ \theta}{a^2}\right)d\theta$$
$$= 6\pi B\int_{-1}^{1}\cos^2\theta d(\cos\ \theta) = 4\pi a^3 K$$
$$= 4\pi a^3\left[a_c\rho_f\left(\frac{\rho_f-\rho_p}{2\rho_p+\rho_f}\right)\right] = V_p\left[3a_c\rho_f\left(\frac{\rho_f-\rho_p}{2\rho_p+\rho_f}\right)\right] \quad (45)$$

3.5. Change in virtual mass of particle due to relative motion

The actual mass of the particle is given by Eq. (8).

The induced mass due to the relative motion of particle and fluid is

$$m_{p,induced}|_{motion} = -\frac{F_{f,z}}{a_c} = -3\rho_f V_p\left(\frac{\rho_f-\rho_p}{2\rho_p+\rho_f}\right) \quad (46)$$

The induced mass due to buoyancy is

$$m_{p,induced}|_{buoyancy} = V_p(\rho_f - \rho_p) \quad (47)$$

This buoyancy is a fictitious inertia force experienced in coordinates fixed to the container. The force is proportional to mass, i.e. it acts like gravity.

The total induced mass (see also Eq. (11) in [3]) is

$$m_{p,induced} = m_{p,induced}|_{motion} + m_{p,induced}|_{buoyancy}$$
$$= -3V_p\rho_f\left(\frac{\rho_f-\rho_p}{2\rho_p+\rho_f}\right) + V_p(\rho_f-\rho_p)$$
$$= -V_p(\rho_f-\rho_p)\left[\frac{3\rho_f}{2\rho_p+\rho_f} - 1\right]$$
$$= -V_p\frac{2(\rho_f-\rho_p)^2}{2\rho_p+\rho_f} \quad (48)$$

In conclusion, the virtual mass of the particle is

$$m_{p,virtual} = m_p + m_{p,induced} = V_p\rho_p - V_p\frac{2(\rho_f-\rho_p)^2}{2\rho_p+\rho_f} = V_p\left[\rho_p - \frac{2(\rho_f-\rho_p)^2}{2\rho_p+\rho_f}\right] \tag{49}$$

3.5.1. Examples of the virtual mass of the particle

Three main cases can be studied.

Example 1. Light particle, e.g. air bubble in water ($\rho_p \ll \rho_f$):

$$\begin{aligned}&\tfrac{2(\rho_f-\rho_p)^2}{2\rho_p+\rho_f} \approx 2\rho_f\\ &m_{p,virtual} \approx V_p(\rho_p - 2\rho_f) \approx -2\rho_f V_p\\ &\rho_{p,virtual} \approx \rho_p - 2\rho_f \approx -2\rho_f\end{aligned} \tag{50}$$

Example 2. Same density ($\rho_p = \rho_f$):

$$\begin{aligned}&\tfrac{2(\rho_f-\rho_p)^2}{2\rho_p+\rho_f} = 0\\ &m_{p,virtual} = \rho_p V_p\\ &\rho_{p,virtual} = \rho_p\end{aligned} \tag{51}$$

Example 3. Heavy particle, e.g. sand particle in water ($\rho_p \gg \rho_f$):

$$\begin{aligned}&\rho_p - \tfrac{2(\rho_f-\rho_p)^2}{2\rho_p+\rho_f} \approx \tfrac{5\rho_f}{2}\\ &m_{p,virtual} \approx \frac{5\rho_f V_p}{2}\\ &\rho_{p,virtual} \approx \frac{5\rho_f}{2}\end{aligned} \tag{52}$$

4. Inviscid particle and viscous fluid: zero particle density

The material in this Section is taken from [16] and included for completeness.

The force on the container is given by

$$F_{f,z} = \oint_{S_f} p_f dS_{f,z} = \oint_{S_p} p_f dS_{p,z} + i\omega\rho_f \oint_{S_p} (ru_{f,r})|_{r=a} dS_{p,z} \tag{53}$$

Here, the task is to derive expressions for p_f and $u_{f,r}$. The equation of the motion for the fluid now includes a viscosity term

$$\begin{aligned}&i\omega\rho_f \bar{u}_f = -\nabla p_f + \mu_f \nabla^2 \bar{u}_f\\ &(\nabla^2 + h^2)\bar{u}_f = \frac{1}{\mu_f}\nabla p_f,\end{aligned} \tag{54}$$

where h is a complex constant [17] and

$$\nu_f = \frac{\mu_f}{\rho_f} \tag{55}$$

Here, ν_f is the kinematic viscosity and μ_f is the dynamic viscosity.

The starting point for the derivation is § 353 in [17]. The near field of the particle is a solution of Eq. (54) with

$$\begin{aligned}&h^2 = -\frac{i\omega\rho_f}{\mu_f}\\ &h = -\frac{1}{\delta}(-1+i)\\ &\delta = \sqrt{\frac{2\mu_f}{\omega\rho_f}},\end{aligned} \tag{56}$$

where δ is the characteristic viscous sub-layer thickness for an oscillatory motion of a liquid near a boundary, see § 24 in [13]. For the situation that we are analyzing, δ is the characteristic thickness of the viscous layer surrounding the particle.

We now define the functions

$$\begin{aligned}&f_0(\zeta) = \tfrac{e^{-i\zeta}}{\zeta}\\ &f_0'(\zeta) = \frac{df_0(\zeta)}{d\zeta} = e^{-i\zeta}\left(\frac{-i\zeta-1}{\zeta^2}\right)\\ &f_2(\zeta) = e^{-i\zeta}\left(-\frac{1}{\zeta^3}+\frac{3i}{\zeta^4}+\frac{3}{\zeta^5}\right)\\ &f_2'(\zeta) = \frac{df_2(\zeta)}{d\zeta} = e^{-i\zeta}\left(\frac{i\zeta+3}{\zeta^4}+\frac{3\zeta-12i}{\zeta^5}+\frac{-3i\zeta-15}{\zeta^6}\right),\end{aligned} \tag{57}$$

where

$$\zeta = ha = -\frac{a}{\delta}(-1+i) \tag{58}$$

The general structure of the equations for pressure and velocity is provided in [17].

Boundary conditions on the surface of the particle lead to

$$\begin{aligned}&\sigma_{rr} = p_{f,0} = \chi_f z = \chi_f r\cos\theta\\ &z|_{r=a,\theta=0} = a\\ &p_f = -p_{f,0}\\ &p_f|_{r=a,\ \theta=0} = -\chi_f a = \rho_f a_c a,\end{aligned} \tag{59}$$

where σ_{rr} is defined in § 15 of [13].

The final result is the expression for the force on the fluid

$$F_{f,z} = -\tfrac{4}{3}\pi a^3 \chi_f F = \tfrac{4}{3}\pi a^3 a_c \rho_f F = \rho_f V_p a_c F, \tag{60}$$

where the reaction force coefficient F is

$$F = 1 + \zeta^2 \frac{-\frac{1}{3}\zeta(2f_0'(\zeta) - \zeta^2 f_2'(\zeta) + \zeta f_2(\zeta)) + 2(f_0(\zeta) + \zeta^2 f_2(\zeta))}{\frac{1}{6}(-\zeta^3 + 12\zeta)(2f_0'(\zeta) - \zeta^2 f_2'(\zeta) + \zeta f_2(\zeta)) + 4\zeta(f_0'(\zeta) + \zeta^2 f_2'(\zeta) + 2\zeta f_2(\zeta))} \tag{61}$$

In Eq. (9) in [4] there is a typographical error in the equation for the F factor: the first ζ-term in the denominator is $-\zeta^2$ instead of $-\zeta^3$.

Note that this expression for F is only a function of ζ, i.e. the Stokes number (see Eq. (58))

$$\frac{a}{\delta} = a\sqrt{\frac{\omega\rho_f}{2\mu_f}} \tag{62}$$

The importance of the Stokes number is also highlighted in [1], where it was found that a large Stokes number implies a higher degree of phase decoupling.

A plot of the real and imaginary parts of F as a function of (a/δ) is shown in Fig. 2 (same as Fig. 4 in [4]).

The real part of F is a virtual mass loss, ranging from the actual mass loss to three times the actual mass loss.

The imaginary part of F represents the damping that acts against the vibrating force. As seen from Fig. 2, the maximum damping occurs at $(a/\delta) = 2.5$.

The virtual mass loss has two limits, one for high viscosity ($F = 1$) and one for low viscosity ($F = 3$).

$$\tfrac{a}{\delta} \to 0 \Rightarrow F \to 1$$

$$F_{f,z} = \rho_f V_p a_c F = \rho_f V_p a_c \tag{63}$$

$$\tfrac{a}{\delta} \to \infty \Rightarrow F \to 3$$

$$F_{f,z} = \rho_f V_p a_c F = 3\rho_f V_p a_c \tag{64}$$

Under the assumption that $\rho_p \ll \rho_f$, the result in Eq. (64) is the same as in Eq. (45).

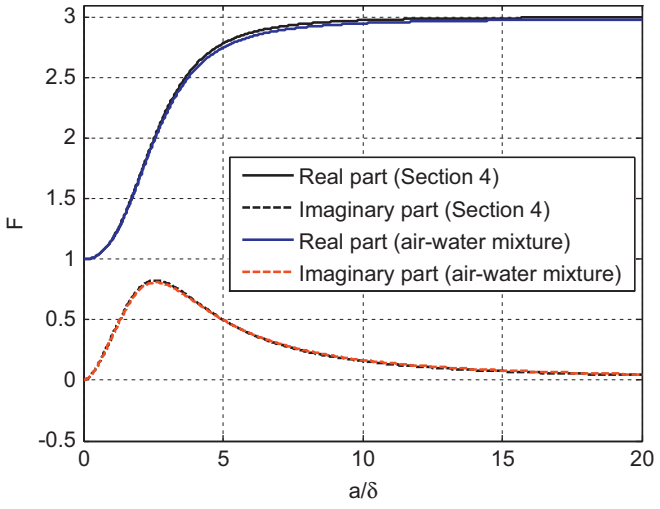

Fig. 2. Real (solid lines) and imaginary (dashed lines) part of the F factor. Black is for the case treated in Section 4: Inviscid particle, viscous fluid and zero particle density. Blue and red is for an air–water mixture. (For interpretation of the references to color in this figure legend, the reader is referred to the web version of this article.)

5. Viscous particle and fluid: finite particle density

The material in this Section is taken from [18] and included for completeness.

The starting point in [18] is a formula for the drag force on a spherical droplet oscillating in a fluid [19].

The force on the fluid is

$$F_{f,z} = (\rho_f - \rho_p) V_p a_c F, \tag{65}$$

where the reaction force coefficient F is

$$F = 1 + \frac{4(1-\tau)}{4\tau - (9iG/\beta^2)} \tag{66}$$

The density ratio is

$$\tau = \frac{\rho_p}{\rho_f} \tag{67}$$

The Stokes number is

$$\beta = \frac{a}{\delta} \tag{68}$$

$$G = 1 + \lambda + \frac{\lambda^2}{9} - \frac{(1+\lambda)^2 f(\lambda)}{\kappa[\lambda^3 - \lambda^2 \tanh\lambda - 2f(\lambda)] + (\lambda+3)f(\lambda)} \tag{69}$$

$$\lambda = (1+i)\beta = \zeta^*, \tag{70}$$

where $\langle\cdot\rangle^*$ denotes the complex conjugate.

$$f(\lambda) = \lambda^2 \tanh\lambda - 3\lambda + 3\tanh\lambda \tag{71}$$

The viscosity ratio is

$$\kappa = \frac{\mu_p}{\mu_f} \tag{72}$$

5.1. Examples of mixtures

To illustrate Eq. (66), we treat three examples of mixtures, with water as the fluid.

The particles considered are air, heavy oil and sand, see Table 2 for the material properties used; c is the speed of sound.

For heavy oil, we use properties from [20].

For sand, we use the density and speed of sound of transparent fused silica [21]. For modeling purposes we can assume that the dynamic viscosity of sand is very large (infinite).

The corresponding density and viscosity ratios are shown in Table 3.

The reaction force coefficient for these mixtures is shown in Fig. 2 (air–water), Fig. 3 (oil–water) and Fig. 4 (sand–water).

The real part of $F(a/\delta = 20)$ is 3 for the air–water mixture, 1.1 for the oil–water mixture and 0.6 for the sand–water mixture.

6. Measurement errors

We now proceed to the derivation of measurement errors based on the previous results.

The particles are all assumed to have the same radius and to be non-interacting, i.e. not too close to each other. We also assume that the particles are homogeneously dispersed throughout the fluid. The assumption that we can neglect gravity effects is also needed to treat the particles as uniformly distributed in the fluid.

Table 2
Material properties for air, heavy oil, water and sand.

Room temperature atmospheric pressure	ρ $\left[\frac{kg}{m^3}\right]$	μ $\left[\frac{kg}{ms}\right]$	c $\left[\frac{m}{s}\right]$
Gas particle (air)	1.2	2e−5	343
Liquid particle (heavy oil)	868	5e−2	1441
Fluid (water)	998	1e−3	1481
Solid particle (sand)	2200	1e12 (∞)	5968 (longitudinal wave)

Table 3
Material ratios and the minimum speed of sound in the mixture.

Room temperature atmospheric pressure	$\tau = \frac{\rho_p}{\rho_f}$	$\kappa = \frac{\mu_p}{\mu_f}$	c_{min} $\left[\frac{m}{s}\right]$
Air–water mixture	1.2e−3	2e−2	24
Oil–water mixture	0.87	50	1441
Sand–water mixture	2.2	1e15 (∞)	1473

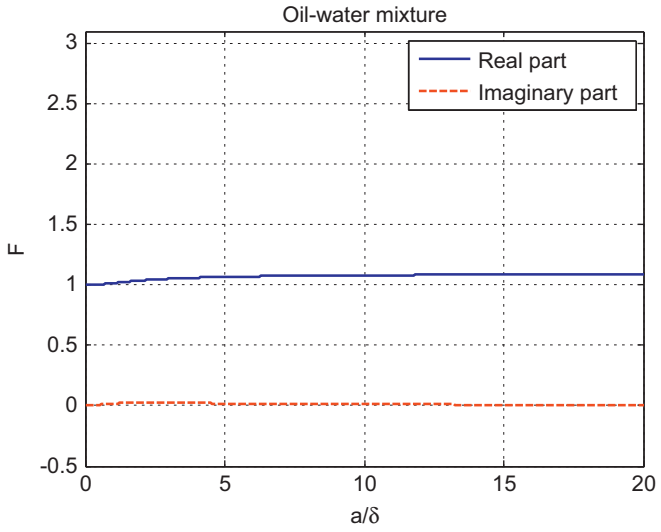

Fig. 3. Real (solid blue line) and imaginary (dashed red line) part of the F factor for an oil–water mixture. (For interpretation of the references to color in this figure legend, the reader is referred to the web version of this article.)

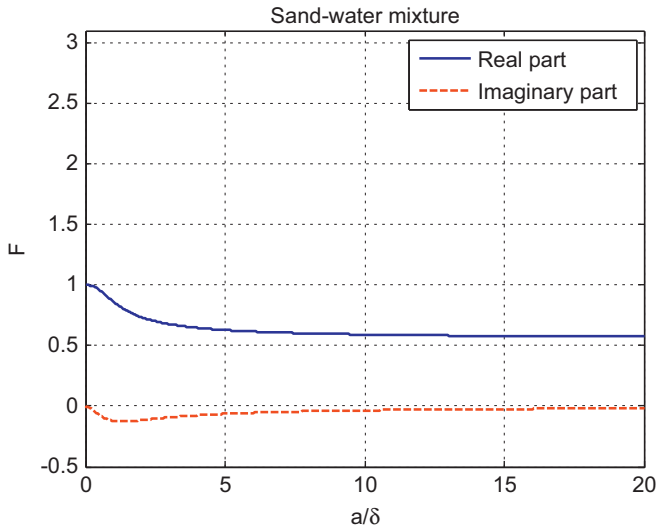

Fig. 4. Real (solid blue line) and imaginary (dashed red line) part of the F factor for a sand–water mixture. (For interpretation of the references to color in this figure legend, the reader is referred to the web version of this article.)

The volumetric particle fraction is defined as

$$\alpha = \frac{V_p}{V_p + V_f} \tag{73}$$

The volumetric particle fraction is assumed to be constant throughout the fluid.

The measurement errors that we plot in the remainder of this paper are shown up to a volumetric particle fraction of 100%. However, due to our assumptions, e.g., that the particles are non-interacting and far from the wall, the measurement errors are most likely only accurate for a volumetric particle fraction below 10%.

6.1. Inviscid particle and viscous fluid: zero particle density

Measurement errors for the case of zero particle density and a viscous (or inviscid) fluid are presented in [4].

The pipe (container) volume considered can be expressed as

$$V_{f-p} = V_p + V_f = A\ell, \tag{74}$$

where A is the pipe cross-sectional area and ℓ is the length of any short length of the flowmeter pipe which is vibrating transversely.

So we can write

$$\alpha = \frac{V_p}{V_{f-p}} \tag{75}$$

and

$$1-\alpha = \frac{V_f}{V_{f-p}} \tag{76}$$

The mass and density of the mixture (we assume $\rho_p = 0$) is

$$m_{f-p} = m_f + m_p = m_f = \rho_f V_f$$
$$\rho_{f-p} = \alpha\rho_p + (1-\alpha)\rho_f = (1-\alpha)\rho_f \tag{77}$$

The mass flow rate of the mixture is

$$\dot{m}_{f-p} = \rho_{f-p} A v = \rho_f A(1-\alpha)v, \tag{78}$$

where

$$v = v_p = v_f \tag{79}$$

is the mean flow speed. We assume that there is no particle slip velocity, i.e., the particle and the fluid move at the same velocity. We also assume plug flow.

We assume that the angular oscillation frequency ω is sufficiently fast so that the flow does not move appreciably during one cycle of the vibration.

The total inertia reaction force on the pipe section is the sum of the force due to the liquid with mass $m_f = \rho_f V_{f-p}$ and due to the particle

$$\begin{aligned} F_m &= -\rho_f V_{f-p} a_c + F_{f,z} \\ &= -\rho_f V_{f-p} a_c + \rho_f V_p a_c F \\ &= -\rho_f V_{f-p}\left(1 - \frac{V_p}{V_{f-p}}F\right) a_c \\ &= -\rho_f V_{f-p}(1-\alpha F) a_c \end{aligned} \tag{80}$$

Therefore, the force per unit length of pipe is

$$\frac{F_m}{\ell} = -\rho_f A(1-\alpha F)a_c = -\rho_f A_m a_c, \tag{81}$$

where we have defined an effective area for inertia

$$A_m = A(1-\alpha F) \tag{82}$$

The apparent density measured is

$$\rho_a = \rho_f(1-\alpha F) \tag{83}$$

The apparent mass flow rate measured is

$$\dot{m}_a = \rho_f A(1-\alpha F)v \tag{84}$$

Now we can calculate the density error (Fig. 5)

$$E_d = \frac{\rho_a - \rho_{f-p}}{\rho_{f-p}} = -\alpha F \tag{85}$$

and the mass flow rate error (Fig. 6)

$$E_{\dot{m}} = \frac{\dot{m}_a - \dot{m}_{f-p}}{\dot{m}_{f-p}} = \frac{\rho_f A(1-\alpha F)v - \rho_f A(1-\alpha)v}{\rho_f A(1-\alpha)v} = \frac{\alpha(1-F)}{(1-\alpha)} \tag{86}$$

We note that these errors are calculated based on the assumption that the flowmeter is supposed to measure the density and mass flow rate of the fluid phase, see Appendix A in [2].

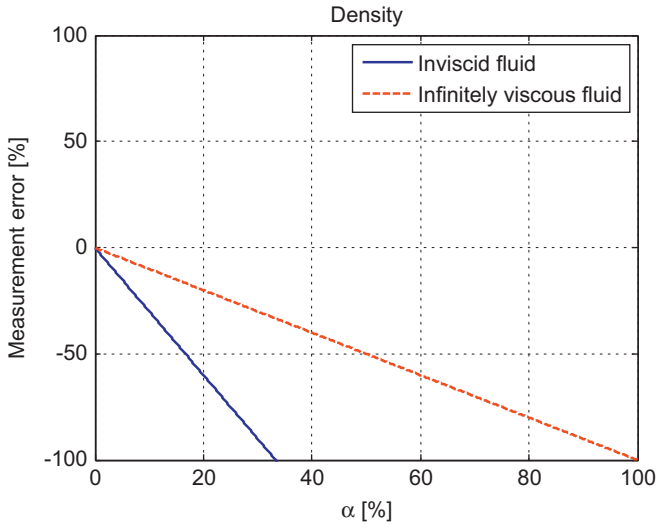

Fig. 5. Density measurement error based on zero particle density: solid blue line for an inviscid fluid, dashed red line for an infinitely viscous fluid. (For interpretation of the references to color in this figure legend, the reader is referred to the web version of this article.)

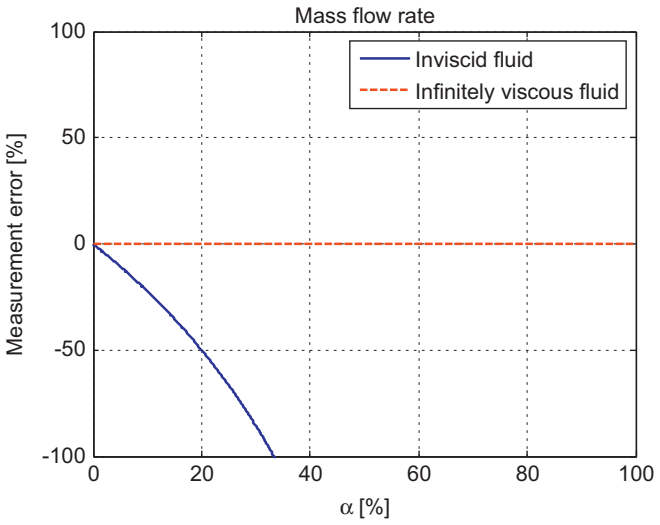

Fig. 6. Mass flow rate measurement error based on zero particle density: solid blue line for an inviscid fluid, dashed red line for an infinitely viscous fluid. (For interpretation of the references to color in this figure legend, the reader is referred to the web version of this article.)

For the infinitely viscous case, the density error is always negative and there is no mass flow rate error.

For the inviscid case, both density and mass flow rate errors are negative. They intersect at

$$E_d = E_{\dot m}$$

$$\alpha = \frac{1}{3} \tag{87}$$

So if the particle fraction is less than 33%, the largest error is in the density measurement. For a particle fraction of more than 33%, the largest error is in the mass flow rate measurement.

6.2. Viscous particle and fluid: finite particle density

We now repeat the steps from Section 6.1 but replacing $F_{f,z}$ (Eq. (60)) by $F_{f,z}$ (Eq. (65)).

The total inertia reaction force on the pipe section is

$$\begin{aligned} F_m &= -\rho_f V_{f-p} a_c + F_{f,z} \\ &= -\rho_f V_{f-p} a_c + (\rho_f - \rho_p) V_p a_c F \\ &= -\rho_f V_{f-p} \left[1 - \frac{V_p}{V_{f-p}} F \left(\frac{\rho_f - \rho_p}{\rho_f}\right)\right] a_c \\ &= -\rho_f V_{f-p} \left[1 - \alpha F \left(\frac{\rho_f - \rho_p}{\rho_f}\right)\right] a_c \end{aligned} \tag{88}$$

The force per unit length of pipe is

$$\frac{F_m}{\ell} = -\rho_f A \left[1 - \alpha F \left(\frac{\rho_f - \rho_p}{\rho_f}\right)\right] a_c = -\rho_f A_m a_c \tag{89}$$

The effective area for inertia is

$$A_m = A \left[1 - \alpha F \left(\frac{\rho_f - \rho_p}{\rho_f}\right)\right] \tag{90}$$

The apparent density measured is

$$\rho_a = \rho_f \left[1 - \alpha F \left(\frac{\rho_f - \rho_p}{\rho_f}\right)\right] \tag{91}$$

The apparent mass flow rate measured is

$$\dot m_a = \rho_f A \left[1 - \alpha F \left(\frac{\rho_f - \rho_p}{\rho_f}\right)\right] v \tag{92}$$

Now we can calculate the density error

$$\begin{aligned} E_d &= \frac{\rho_a - \rho_{f-p}}{\rho_{f-p}} \\ &= \frac{\rho_f \left[1 - \alpha F \left(\frac{\rho_f - \rho_p}{\rho_f}\right)\right] - [\alpha\rho_p + (1-\alpha)\rho_f]}{\alpha\rho_p + (1-\alpha)\rho_f} \\ &= \frac{\alpha(\rho_f - \rho_p)(1-F)}{\alpha\rho_p + (1-\alpha)\rho_f} \end{aligned} \tag{93}$$

and the mass flow rate error

$$\begin{aligned} E_{\dot m} &= \frac{\dot m_a - \dot m_{f-p}}{\dot m_{f-p}} \\ &= \frac{\rho_f A \left[1 - \alpha F \left(\frac{\rho_f - \rho_p}{\rho_f}\right)\right] v - A[\alpha\rho_p + (1-\alpha)\rho_f] v}{A[\alpha\rho_p + (1-\alpha)\rho_f] v} \\ &= \frac{\alpha(\rho_f - \rho_p)(1-F)}{\alpha\rho_p + (1-\alpha)\rho_f} \end{aligned} \tag{94}$$

We observe that

$$E_{\dot m} = E_d \tag{95}$$

We note that these errors are calculated based on the assumption that the flowmeter is supposed to measure the density and mass flow rate of the mixture. This is in contrast to the error calculations in Section 6.1.

If the particle and fluid density are equal, the error is zero.

There are two limiting cases for the errors. The first is where the particle density is low compared to the fluid density

$$\begin{aligned} &\rho_p \ll \rho_f \\ &E_{\dot m} = E_d \approx \tfrac{\alpha(1-F)}{1-\alpha} \end{aligned} \tag{96}$$

The second is where the particle density is high compared to the fluid density

$$\begin{aligned} &\rho_p \gg \rho_f \\ &E_{\dot m} = E_d \approx F - 1 \end{aligned} \tag{97}$$

Errors for the three mixtures introduced in Section 5.1 are shown in Fig. 7.

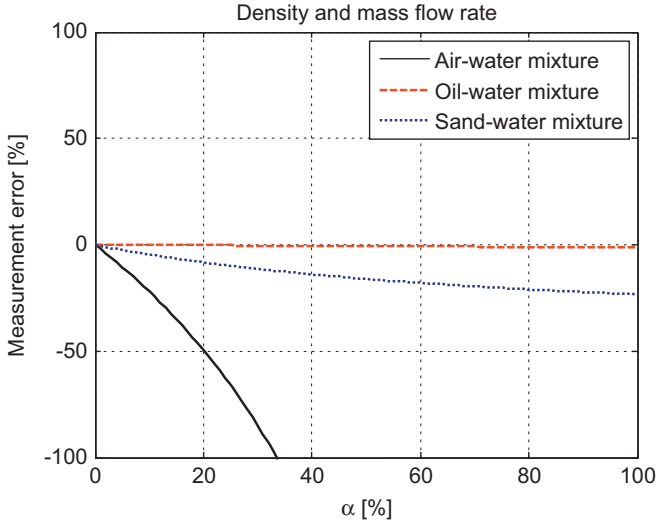

Fig. 7. Density and mass flow rate error for mixtures: air–water (solid black line), oil–water (dashed red line) and sand–water (dotted blue line). (For interpretation of the references to color in this figure legend, the reader is referred to the web version of this article.)

7. Compressibility errors

Density and mass flow rate measurement errors due to compressibility effects have been derived in [2]

$$E_d = \frac{1}{4}\left(\frac{\omega}{c_{f-p}}b\right)^2$$

$$E_{\dot{m}} = 2E_d = \frac{1}{2}\left(\frac{\omega}{c_{f-p}}b\right)^2, \tag{98}$$

where ω is the driver frequency, c_{f-p} is the mixture speed of sound and b is the pipe radius.

The frequency of the fundamental transverse acoustic mode is [2]

$$f_{FTAM} = \frac{j'_{1,1}c_{f-p}}{2\pi b}, \tag{99}$$

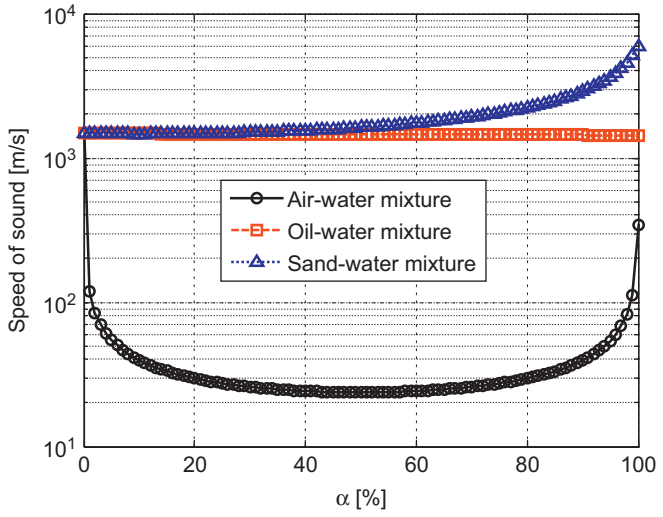

Fig. 8. Speed of sound for mixtures: air–water (solid black line and circles), oil–water (dashed red line and squares) and sand–water (dotted blue line and triangles). Note that the vertical scale is logarithmic. (For interpretation of the references to color in this figure legend, the reader is referred to the web version of this article.)

where $j'_{1,1} = 1.84118$ is the first zero of the derivative of the Bessel function of the first kind of order 1.

Now we introduce the reduced frequency, which is the ratio of the driver frequency and the frequency of the fundamental transverse acoustic mode [5]

$$f_{red} = \frac{f}{f_{FTAM}} = \frac{2\pi bf}{j'_{1,1}c_{f-p}} = \frac{1}{j'_{1,1}}\left(\frac{\omega}{c_{f-p}}b\right) \tag{100}$$

We find that the errors due to compressibility can be expressed using the reduced frequency

$$E_d = \frac{1}{4}\left(\frac{\omega}{c_{f-p}}b\right)^2 = \frac{1}{4}(j'_{1,1}f_{red})^2 = \frac{j'^2_{1,1}}{4}f^2_{red}$$

$$E_{\dot{m}} = 2E_d = \frac{j'^2_{1,1}}{2}f^2_{red} \tag{101}$$

8. Combined compressibility and phase decoupling error

For certain conditions, the errors due to compressibility and phase decoupling can simply be added. We quote from Appendix A in [2]:

"We expect this simple addition of errors to be valid when the individual error contributions are small compared to 1. Then, there should be no physical interaction between the processes of bubble compression (or expansion) and bubble motion relative to the liquid; so these effects can be linearly combined."

When those conditions are fulfilled, the expressions for the combined (or total) error are

$$E_d = \frac{\alpha(\rho_f-\rho_p)(1-F)}{\alpha\rho_p+(1-\alpha)\rho_f} + \frac{1}{4}\left(\frac{\omega}{c_{f-p}}b\right)^2$$

$$E_{\dot{m}} = \frac{\alpha(\rho_f-\rho_p)(1-F)}{\alpha\rho_p+(1-\alpha)\rho_f} + \frac{1}{2}\left(\frac{\omega}{c_{f-p}}b\right)^2 \tag{102}$$

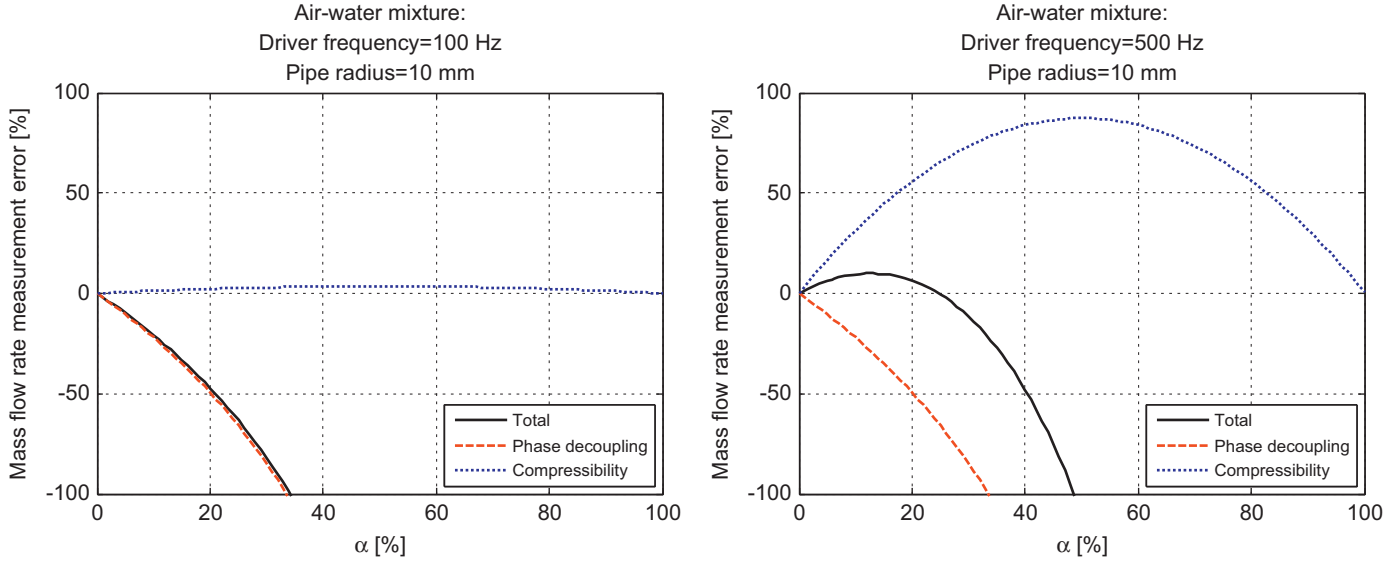

Fig. 9. Mass flow rate error for a mixture of air and water: total error (solid black line), phase decoupling error (dashed red line) and compressibility error (dotted blue line). Left: low driver frequency. Right: high driver frequency. (For interpretation of the references to color in this figure legend, the reader is referred to the web version of this article.)

8.1. Mixture examples

For the calculations, we assume that the driver frequency is independent of α. In reality, the driver frequency increases with decreasing density.

The speed of sound of the mixtures is found using the following formula [22]:

$$\frac{1}{\rho_{f-p}c_{f-p}^2}=\frac{1-\alpha}{\rho_f c_f^2}+\frac{\alpha}{\rho_p c_p^2}$$

$$c_{f-p}=\sqrt{\frac{1}{\rho_{f-p}}\left(\frac{\rho_f c_f^2 \rho_p c_p^2}{\rho_p c_p^2(1-\alpha)+\rho_f c_f^2 \alpha}\right)} \tag{103}$$

The speed of sound of the mixtures is shown in Fig. 8. The minimum speed of sound for the mixtures can be found in Table 3.

We now calculate the combined error for a pipe radius of 10 mm. Two different driver frequencies are considered, low frequency (100 Hz) and high frequency (500 Hz).

The corresponding mass flow rate error for the air–water mixture is shown in Fig. 9. For the low frequency, the error due to phase decoupling dominates. For the high frequency, the compressibility error becomes important and makes the total error positive up to a high particle fraction. A similar overall behavior is found for the density error of the air–water mixture, see Fig. 10. The only difference is that the magnitude of the compressibility error is half of that for the mass flow rate. The consequence of this difference is that the total error is negative for all particle fractions.

Different error behavior is observed for the oil–water and sand–water mixtures, see Figs. 11 and 12: For both low and high driver frequencies, the error due to phase decoupling dominates. The reason is that the mixture speed of sound is very high.

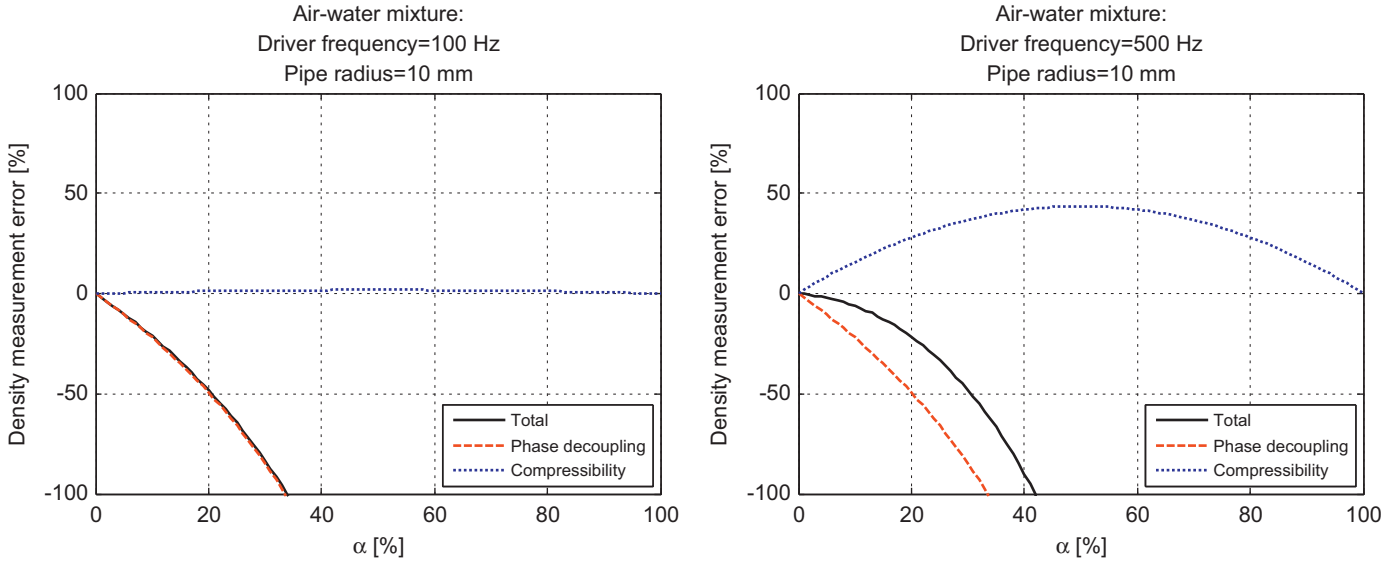

Fig. 10. Density error for a mixture of air and water: total error (solid black line), phase decoupling error (dashed red line) and compressibility error (dotted blue line). Left: low driver frequency. Right: high driver frequency. (For interpretation of the references to color in this figure legend, the reader is referred to the web version of this article.)

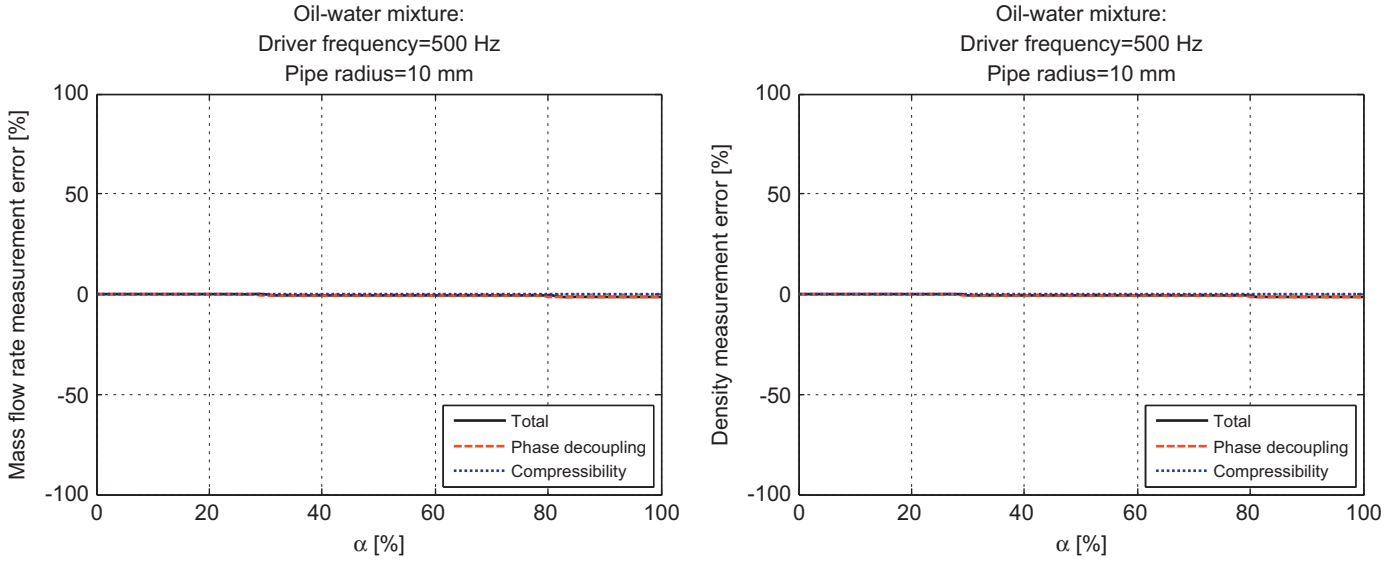

Fig. 11. Measurement error at high driver frequency for a mixture of oil and water: total error (solid black line), phase decoupling error (dashed red line) and compressibility error (dotted blue line). Left: mass flow rate. Right: density. (For interpretation of the references to color in this figure legend, the reader is referred to the web version of this article.)

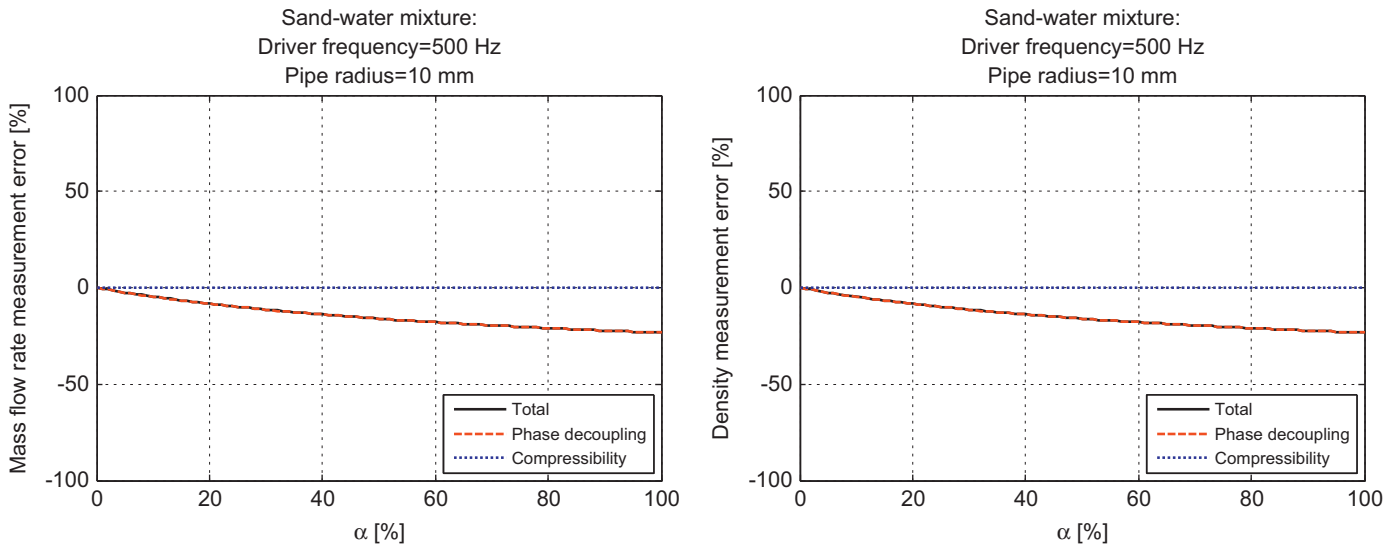

Fig. 12. Measurement error at high driver frequency for a mixture of sand and water: total error (solid black line), phase decoupling error (dashed red line) and compressibility error (dotted blue line). Left: mass flow rate. Right: density. (For interpretation of the references to color in this figure legend, the reader is referred to the web version of this article.)

Table 4
Bubble theory assumptions.

Part of system	Assumptions
Overall	• The effect of gravity is neglected
Flow (particles and fluid)	• Particles and fluid move at the same velocity • Particles homogeneously dispersed in fluid • Plug flow • Incompressible
Particles	• Sphere • Surface tension is not taken into account • Single radius • Non-interacting
Container	• Rigid (no fluid-structure interaction) • Oscillation amplitude is small compared to the particle radius • Oscillation frequency: Fast compared to the flow speed Independent of the volumetric particle fraction
Particles and container	• The particle is far from wall of the container (the particle size is small relative to the size of the container)

9. Discussion

9.1. Main bubble theory assumptions

The assumptions underlying the bubble theory are scattered throughout the paper. It may be useful for the reader to have an overview of the main assumptions; these are collected in Table 4.

9.2. Other important effects not included

A constant volumetric particle fraction α is assumed in the flowmeter. This implies that there is no pressure loss between the flowmeter inlet and outlet.

The pipe geometry is not taken into account. One could imagine that particles are trapped in certain locations of the flowmeter if it is not a single straight pipe.

The flow pattern is not modeled, e.g. particle coalescing and breakup. This is most important for low flow speeds where it cannot be assumed that particles are homogeneously dispersed in the fluid.

It is likely that there is interplay between the above-mentioned effects.

10. Conclusions

In this paper we have reviewed the "bubble theory". A combination of published and unpublished papers has been used to outline the structure of the theory. The main result is the force on an oscillating fluid due to a particle (Eq. (65)). This force can be used to derive an expression for the measurement error due to phase decoupling (Eqs. (93) and (94)). The total error due to (i) phase decoupling and (ii) compressibility is provided in Eq. (102).

The results have been illustrated using examples where water (the fluid) is mixed with air, oil and sand (the particle).

Acknowledgments

The author is grateful to Dr. John Hemp for useful discussions and for providing the major part of the derivation in Section 3 [15] along with [16,18].

References

[1] Weinstein JA. The motion of bubbles and particles in oscillating liquids with applications to multiphase flow in Coriolis meters. Boulder, Colorado, USA: University of Colorado; 2008.
[2] Hemp J, Kutin J. Theory of errors in Coriolis flowmeter readings due to compressibility of the fluid being metered. Flow Meas Instrum 2006;17:359–69.
[3] Hemp J, Sultan G. On the theory and performance of Coriolis mass flowmeters. In: Proceedings of the international conference on mass flow measurement, IBC technical services; 1989. p. 1–38.
[4] Hemp J, Yeung H, Kassi L. Coriolis meter in two phase conditions. IEE one-day seminar; 2003. p. 1–13.
[5] Gysling DL. An aeroelastic model of Coriolis mass and density meters operating on aerated mixtures. Flow Meas Instrum 2007;18:69–77.

[6] Zhu H. Application of Coriolis mass flowmeters in bubbly or particulate two-phase flows. Erlangen and Nuremberg, Germany: University of Erlangen-Nuremberg; 2008.
[7] Thomsen JJ, Dahl J. Analytical predictions for vibration phase shifts along fluid-conveying pipes due to Coriolis forces and imperfections. J Sound Vibr 2010;329:3065–81.
[8] Enz S, Thomsen JJ, Neumeyer S. Experimental investigation of zero phase shift effects for Coriolis flowmeters due to pipe imperfections. Flow Meas Instrum 2011;22:1–9.
[9] Kutin J, Hemp J, Bobovnik G, Bajsic I. Weight vector study of velocity profile effects in straight-tube Coriolis flowmeters employing different circumferential modes. Flow Meas Instrum 2005;16:375–85.
[10] Kutin J, Bobovnik G, Hemp J, Bajsic I. Velocity profile effects in Coriolis mass flowmeters: recent findings and open questions. Flow Meas Instrum 2006;17:349–58.
[11] Henry M, Tombs M, Duta M, Zhou F, Mercado R, Kenyery F, et al. Two-phase flow metering of heavy oil using a Coriolis mass flow meter: a case study. Flow Meas Instrum 2006;17:399–413.
[12] Henry M, Tombs M, Zamora M, Zhou F. Coriolis mass flow metering for three-phase flow: a case study. Flow Meas Instrum 2013;30:112–22.
[13] Landau LD, Lifshitz EM. Fluid mechanics. 2nd ed. Oxford, UK: Elsevier/Butterworth-Heinemann; 1987.
[14] Panton RL. Incompressible flow. 3rd ed. Hoboken, New Jersey, USA: Wiley; 2005.
[15] Hemp J. Private communication; 2013 and 2014.
[16] Hemp J. Reaction force due to a small bubble in a liquid filled container undergoing simple harmonic motion; 2003. p. 1–21. Unpublished.
[17] Lamb H. Hydrodynamics. 6th ed. Cambridge, UK: Cambridge University Press; 1932.
[18] Hemp J. Reaction force of a bubble (or droplet) in a liquid undergoing simple harmonic motion; 2003. p. 1–13. Unpublished.
[19] Yang S-M, Leal LG. A note on memory-integral contributions to the force on an accelerating spherical drop at low Reynolds number. Phys Fluids A 1991;3:1822–4.
[20] Kalivoda RJ. Understanding the limits of ultrasonics for crude oil measurement. ⟨http://www.fmctechnologies.com⟩. [Online] ⟨http://www.fmctechnologies.com/en/MeasurementSolutions/BusinessHighlights/~/media/AMeasurement/BusinessHighlightPDFs/FMC_Intl%20Oil%20Gas%20Eng%20Aug_2011.ashx⟩; 2011.
[21] Kaye and Laby; 2014. [Online] ⟨http://www.kayelaby.npl.co.uk⟩.
[22] Wood AB. A textbook of sound. 3rd ed. London, UK: G. Bell & Sons; 1955.